

Electron transport in open systems from finite-size calculations: Examination of the principal layer method applied to linear gold chains

Ariana Beste, Vincent Meunier, and Robert J. Harrison

Citation: *The Journal of Chemical Physics* **128**, 154713 (2008); doi: 10.1063/1.2905219

View online: <https://doi.org/10.1063/1.2905219>

View Table of Contents: <http://aip.scitation.org/toc/jcp/128/15>

Published by the [American Institute of Physics](#)

PHYSICS TODAY

WHITEPAPERS

ADVANCED LIGHT CURE ADHESIVES

Take a closer look at what these environmentally friendly adhesive systems can do

READ NOW

PRESENTED BY
 **MASTERBOND**
ADHESIVES | SEALANTS | COATINGS

Electron transport in open systems from finite-size calculations: Examination of the principal layer method applied to linear gold chains

Ariana Beste,^{1,a)} Vincent Meunier,^{1,2} and Robert J. Harrison^{1,3}

¹Computer Science and Mathematics Division, Oak Ridge National Laboratory, Bethel Valley Road, Oak Ridge, Tennessee 37831-6367, USA

²Center for Nanophase Materials Sciences Division, Oak Ridge National Laboratory, Bethel Valley Road, Oak Ridge, Tennessee 37831, USA

³Department of Chemistry, University of Tennessee, Knoxville, Tennessee 37996, USA

(Received 25 January 2008; accepted 12 March 2008; published online 18 April 2008)

We describe the occurrence of computational artifacts when the principal layer method is used in combination with the cluster approximation for the calculation of electronic transport properties of nanostructures. For a one-dimensional gold chain, we observe an unphysical band in the band structure. The artificial band persists for large principal layers and for large buffer sizes. We demonstrate that the assumption of equality between Hamiltonian elements of neighboring layers is no longer valid and that a discontinuity is introduced in the potential at the layer transition. The effect depends on the basis set. When periodic boundary conditions are imposed and the k -space sampling is converged, the discontinuity disappears and the principal layer method can be correctly applied by using a linear combination of atomic orbitals as basis set. © 2008 American Institute of Physics. [DOI: 10.1063/1.2905219]

INTRODUCTION

Electron transport through nanoscale molecular devices is a research area which faces challenges in both experiment and theory. Experimentally, it is difficult to manipulate and to measure the atomic structure of the electrode-molecule-electrode system. Theoretically, the description of molecular conduction is complicated by the system being open, and not in equilibrium when voltage is applied. Electrical transport properties of organic molecules attached to gold electrodes through thiol end groups have received particular interest¹⁻³ triggered by an early break-junction experiment by Reed *et al.*⁴ In molecular transport theory, the Green's function or direct scattering approaches are combined with the extended Hückel tight-binding theory⁵⁻⁷ or density functional theory (DFT).⁸⁻¹⁴ Generally, even though experimental current-voltage characteristics can be qualitatively reproduced, the magnitude of the computed conductance is typically orders of magnitude too high. Different explanations for this discrepancy are invoked. First, the conductance has been found to strongly depend on the relative position of the Fermi energy of the metal with respect to the molecular levels and the spatial profile of the electrostatic potential under an applied bias.^{7,15-18} Second, charge transfer can be very important.¹⁰ Third, the details of the geometry of the device dramatically influence the conductance. For instance, different contact geometries^{13,8} and tilting angles between molecule and surface^{12,13,19,20} have shown to yield a range of different transport properties. Also, the possibility that the molecule covalently binds to only one side of the surface and the current is mediated through molecule-molecule interactions was

considered.^{21,22} The discussion in the literature is not without controversy¹³ and neither are the detailed electronic structure of the device nor the validity of the applied theoretical methods (i.e., weak coupling regime as treated by DFT).²³⁻²⁹

The theoretical description of molecular transport employing Landauer's formalism³⁰ has been approached by using scattering theory, pioneered by Lang.³¹ A popular alternative is based on the nonequilibrium Green's function (NEGF) method applied to molecular devices by Datta³² and Mujica *et al.*^{33,34} Combining the NEGF with conventional DFT methods used in quantum chemistry or solid state physics provides a tool for determining molecular transport properties from first principles. On the one hand, periodic boundary conditions can be adopted,^{35,36,38} where large parts of the leads are included to avoid the interaction of the molecule with its images. On the other hand, common quantum chemistry codes can be used when the cluster approximation is introduced.^{9-11,18} The extended molecule has to be chosen large enough to accommodate the effects of charge transfer introduced by the molecule-electrode interactions. The same cluster approximation has also been implemented in the NWCHEM program package,³⁷ as described in Refs. 39-41.

Here, we use the NWCHEM-based implementation in conjunction with the CRYSTAL package⁴⁶ to test the cluster approximation in the case of a gold nanowire. The implementation was tested for carbon nanotube systems yielding electronic properties in close agreement with published results.^{39,42} For carbon sp^2 bonded systems a modest basis set is sufficient to reproduce all the salient features of the system near the Fermi level. However, in a metallic, one-dimensional system the slow decay of the potential in combination with the diffuse basis functions can cause a computational artifact. This artifact is explained and we show how to circumvent it.

^{a)} Author to whom correspondence should be addressed. Oak Ridge National Laboratory, P.O. Box 2008, MS 6367, Oak Ridge, TN 37831-6367. Electronic mail: bestea@ornl.gov. Tel.: 865-241-3160. FAX: 865-574-0680.

METHOD AND IMPLEMENTATION

The general theory of transport in molecular electronic devices using NEGF in combination with DFT is well established.^{33,43,44} In summary, a molecular electronic device consists of a conductor C , the “extended” molecule or “active region,” which is coupled to two semi-infinite leads (R and L). Within the Landauer formalism,³⁰ which describes transport through noninteracting systems, the conductance is proportional to the transmission function T . The transmission function is related to the retarded and advanced Green’s functions of the conductor \mathbf{G}_C^r and \mathbf{G}_C^a by

$$T = \text{Tr}[\Gamma_L \mathbf{G}_C^r \Gamma_R \mathbf{G}_C^a], \quad (1)$$

where Γ_L and Γ_R describe the coupling to the leads. All quantities are expressed in a localized basis set and the equations are given in matrix form. The Green’s function of the conductor can be obtained by partitioning the Green’s function of the entire system $(ES - \mathbf{H})\mathbf{G}(E) = \mathbf{I}$ (\mathbf{I} is the identity matrix, \mathbf{H} is the Hamiltonian, \mathbf{S} is the overlap matrix, and E is the energy) which in a localized basis set yields

$$\mathbf{G}_{CC}(E) = \{\mathbf{E}\mathbf{S}_{CC} - [\mathbf{H}_{CC} + \Sigma_L(E) + \Sigma_R(E)]\}^{-1}, \quad (2)$$

with $\Sigma_L(E)$ and $\Sigma_R(E)$ being the self-energies of the semi-infinite left and right leads. The Γ matrices in Eq. (1) are defined through the self-energies of the leads

$$\Gamma_L = i[\Sigma_L - \Sigma_L^\dagger], \quad \Gamma_R = i[\Sigma_R - \Sigma_R^\dagger]. \quad (3)$$

In a localized basis, the description of the leads can be simplified by applying an effective layer concept.⁴⁴ The semi-infinite leads are treated as stacks of principal layers that only interact with their nearest neighbors.⁴⁵ Projecting $(E - H)G(E) = I$ onto Bloch states that are composed of orbitals centered on the atoms forming the layer, results in a hierarchy of equations of the form

$$(\mathbf{E}\mathbf{S}_{00} - \mathbf{H}_{00})\mathbf{G}_{n0} = \mathbf{H}_{01}^\dagger \mathbf{G}_{n-1,0} + \mathbf{H}_{01} \mathbf{G}_{n+1,0}, \quad (4)$$

where the indices refer to the layer number n and for $n=0$ $\mathbf{H}_{01}^\dagger \mathbf{G}_{n-1,0} = \mathbf{I}$. The layers are chosen such that $\mathbf{H}_{00} = \mathbf{H}_{11} = \dots$ and $\mathbf{H}_{01} = \mathbf{H}_{12} = \dots$.

The Hamiltonian and overlap matrices of the conductor, the lead principal layer, and the interaction matrices between layers (\mathbf{H}_{01} and \mathbf{S}_{01}) are required as input for the transport code and are provided by a quantum chemistry program package, for instance. Here, we used the NWCHEM (Ref. 37) and the CRYSTAL (Ref. 46) program packages. While both packages solve the same DFT equations and make use of the atomic orbitals as basis sets, the former is designed for finite-size systems (cluster approximation), while the latter applies adequate boundary conditions to compute the properties of periodic systems.

As a seemingly simple example, we studied the decay of conductance of a one-dimensional gold chain as a gap of different length is introduced. Figure 1 shows a typical input geometry for the quantum chemistry code. The system is

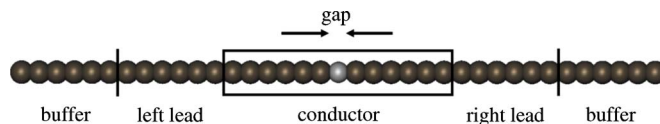


FIG. 1. (Color online) Typical input structure for the quantum chemical code of a gold chain where a gap is introduced.

divided into a conductor region, a left and right lead, and buffer zones on each end. The assumption is that the principal layer is large enough so that only the nearest neighboring layers interact (principal layer condition). This assumption can be verified by increasing the principal layer size and checking for convergence. The buffer zones should have at least the same size as the principal layer to ensure that all the atoms within the principal layer are embedded in the same environment. For the same reason, the conductor region should include at least one principal layer on each side of the molecule (the gap in our case). If bulk calculations were performed, the system was set up similarly than in Fig. 1 where the left lead is directly connected to the right lead.

We employed the local density approximation, the Slater exchange,⁴⁷ and the VWN correlation⁴⁸ functional. The interatomic distance between the gold atoms was fixed to 2.56 Å (an average value of the atomic distances of an optimized gold chain). We used the LANL2DZ effective core potential (ECP) and basis set in two different flavors. The LANL2DZ basis set as implemented in CRYSTAL has a less diffuse exponent for the most diffuse s function, lacks the most diffuse p function, and one p function (composed of two primitives) is decontracted compared to the LANL2DZ basis set implemented in NWCHEM. The former will be denoted as LANL2DZ-cry, the latter as LANL2DZ-nw. The corresponding ECPs for gold are small core ECPs with 60 electrons in the core region and 19 valence electrons. The size of the gap introduced in the gold chain is given as fractions of the gold-gold distance of 2.56 Å (denoted as “ad” below). For a gap size of 0.5 ad and larger, we placed a ghost atom (a full set of basis functions of the gold atom) at the center of the gap. The results shown here have been obtained within a spin-restricted formulation (the results were verified using unrestricted DFT).

RESULTS AND DISCUSSION

First, we investigated the “bulk” properties of a gold chain (i.e., chain without defect) using the LANL2DZ-nw basis. We found that a principal layer size of six gold atoms was converged [see Fig. 2(a)]. However, we observed that the number of open channels at the Fermi energy was two in contradiction with Ref. 49, where a conductance of one quantum unit was determined.

With a principal layer size of six gold atoms we calculated the conductance of gold chains starting with a conductor consisting of 12 gold atoms at equal distance and continuing by placing a gap of increasing size in the middle of the chain. Figure 2(b) shows the results. With increasing gap size, the conductance at the Fermi energy should decrease, reaching a conductance of zero for sufficiently large gaps. Instead, the conductance approaches $0.6G_0$. Also note that

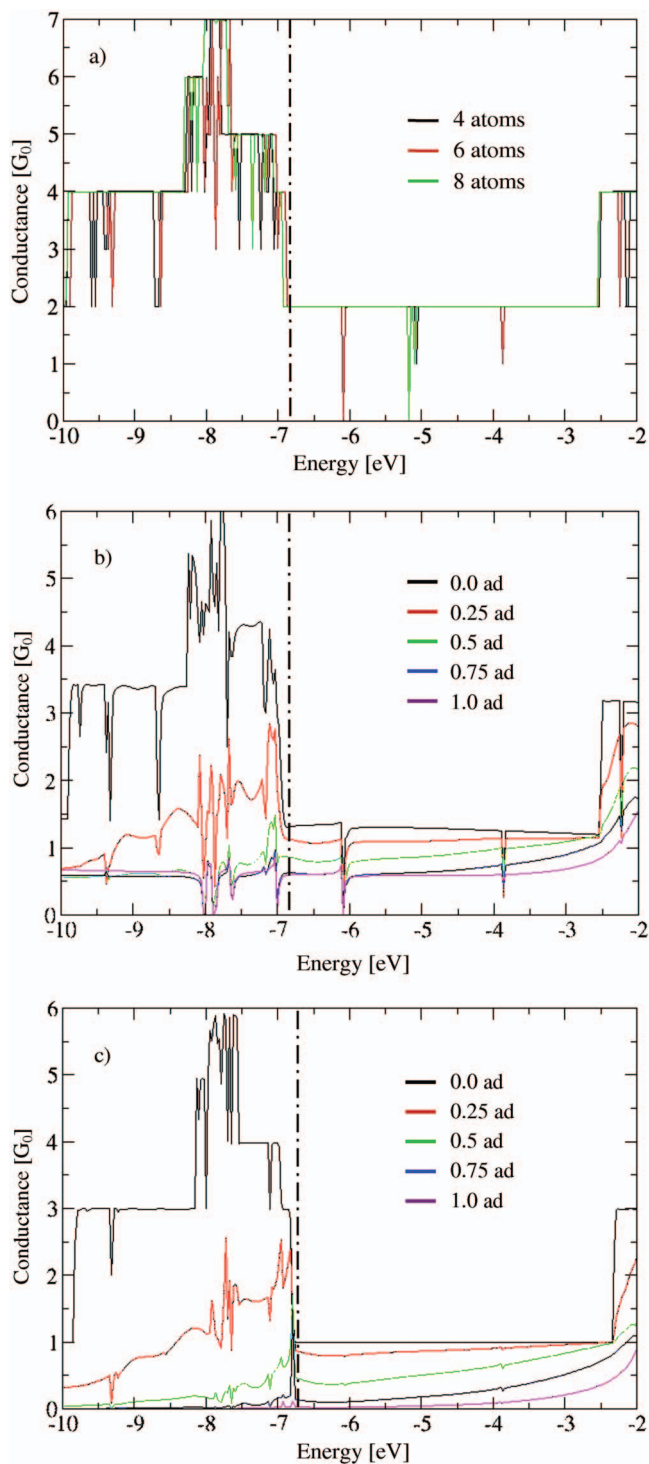


FIG. 2. (Color) Conductance of gold chain, dotted-dashed line denotes Fermi energy. (a) Bulk calculation for different principal layer sizes, LANL2DZ-nw basis set. (b) Conductor calculation for different gap sizes in atomic distances (ad), principal layer size six atoms, LANL2DZ-nw basis set. (c) Conductor calculation for different gap sizes in atomic distances (ad), principal layer size six atoms, LANL2DZ-cry basis set.

for zero gap size the conductance in Fig. 2(b) is lower than the bulk conductance in Fig. 2(a). Figure 2(b) shows gap sizes for up to one atomic distance. We repeated the calculations with gap sizes of two and three atomic distances and found that once the conductance of $0.6G_0$ is reached, the value does not depend on the gap size. Surprisingly, when we

used a slightly different basis set (LANL2DZ-cry), the conductance correctly approaches zero which was reached for a gap size of as small as one atomic distance [Fig. 2(c)]. Also, with the LANL2DZ-cry basis set, the conductance at the Fermi energy for the uninterrupted gold chain is one, which coincides with the conductance bulk calculation using the LANL2DZ-cry basis set.

To investigate this behavior, we calculated the band structure of the gold chain by using the principal layer method for the two basis sets and compared to a band structure calculation using the CRYSTAL program package.⁴⁶ For the CRYSTAL calculation, a $4 \times 1 \times 1$ Monkhorst-Pack⁵⁰ grid is chosen to sample the k space. The unit cell contains six gold atoms which allows for direct comparison to the band structure calculated with the principal layer method using a principal layer consisting of six gold atoms. The band structures are given in Fig. 3. Figure 3 only shows the CRYSTAL band structure calculated with the LANL2DZ-nw basis set, the band structure using the LANL2DZ-cry is very similar. We confirmed that the band structure calculated with the principal layer method using Hamiltonian and overlap matrices from a finite-size calculation coincide with the CRYSTAL band structure for the LANL2DZ-cry basis set [Fig. 3(c)] but for the LANL2DZ-nw basis set [Fig. 3(b)] an additional band appears. Analysis of the band reveals that it is mainly composed of $6p_z$ orbitals (the gold chain is oriented along the z direction). Increasing the principal layer size does not result in the disappearance of the unphysical band; i.e., with a principal layer size of 8, 10, and 12 gold atoms the unphysical band is still present.

Since the artifact in the calculation depends on the choice of the basis set and because the difference in the basis sets lies in the degree of diffuse character in the s and p functions, we first suspected that the principal layer condition is not fulfilled for the more diffuse basis set and that the phenomenological convergence test demonstrated in Fig. 2(a) is not sufficient. The principal layer condition is verified if the Hamiltonian and overlap elements between next nearest layers are negligible. Table I gives the largest Hamiltonian and overlap elements between next nearest layers for different principal layer sizes and the two different basis sets. For the less diffuse basis set (LANL2DZ-cry), the largest absolute values are smaller than 10^{-6} a.u. even when a principal layer of four atoms is used. We find that for a principal layer consisting of six atoms, the Hamiltonian and overlap matrix elements between the next neighbors are very small for either basis set. This indicates that the principal layer condition is fulfilled. For larger principal layers, the absolute values of the matrix elements fall under 10^{-6} a.u. (In Table I, we only included principal layer sizes up to eight atoms but we also checked the matrix elements for principal layer sizes up to twelve atoms.) Despite the fulfillment of the principal layer condition, the artificial band occurred even for principal layer sizes of 8, 10, and 12 gold atoms when the LANL2DZ-nw basis set was used. For the LANL2DZ-cry basis set, the artifact was not found for all tested principal layer sizes (4–12).

Implicit in the derivation of the principal layer method is the assumption that $\mathbf{H}_{00}=\mathbf{H}_{11}=\dots$, $\mathbf{H}_{01}=\mathbf{H}_{12}=\dots$, and similar

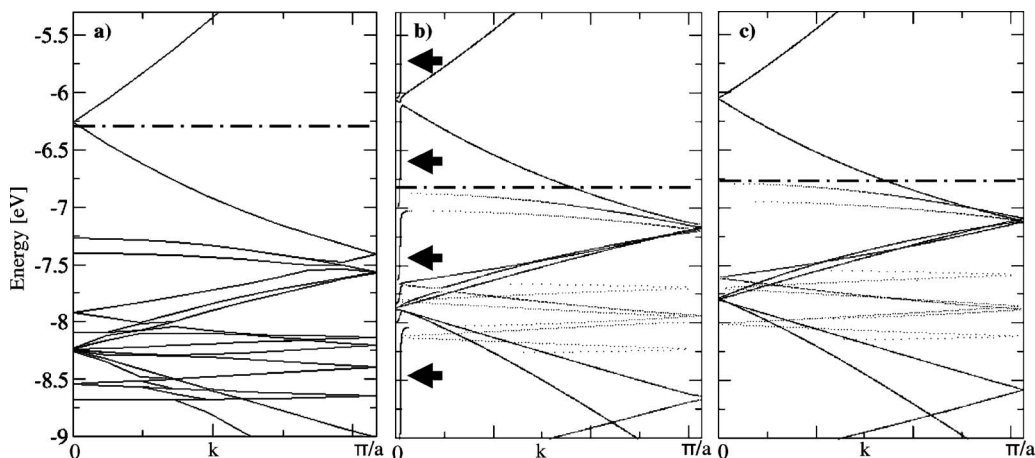


FIG. 3. Band structure of a gold chain, the Fermi level is indicated by a dashed-dotted line. (a) Periodic CRYSTAL calculation, six atoms in unit cell, LANL2DZ-nw. (b) Principal layer method, six atoms in principal layer, LANL2DZ-nw; arrows mark unphysical band. (c) Principal layer method, six atoms in principal layer, LANL2DZ-cry. For transport-based calculations, the bands are represented by dots on the energy grid. This is due to the fact that in that case the bands are expressed as $k(E)$ rather than $E(k)$ since E is an input parameter of the Green's function approach. It follows that some bands might look dotted when the band is flat since step sizes in energy are finite.

for the overlap. In finite-size calculations, as executed within the cluster approximation, the potential experienced by the atoms at the edge of the cluster region is different than that experienced by the atoms within the core region. That does not necessarily mean that above assumption is not fulfilled since we always include a buffer region which is at least the size of the principal layer and assures that there are no direct interaction between the atoms of the principal layer (or the conductor) and the vacuum. However, it might be the source of an inconsistency between the finite-system calculation and the computation of the infinite system which uses the Hamiltonian and overlap matrices of the finite system. Therefore, we compared the band structures calculated with the principal layer method where the input Hamiltonian and overlap matrices are obtained from a finite-size calculation (NWChem) with the band structure calculated with the principal layer method but where the input Hamiltonian and overlap matrices are computed, applying periodic boundary conditions (CRYSTAL). The unit cell in the CRYSTAL calculation contains the same number of atoms as the NWChem input. By using the LANL2DZ-cry basis set, we obtained identical band structures from both the NWChem and CRYSTAL matrix elements. When the LANL2DZ-nw basis set was used, the matrix elements from CRYSTAL reproduced the correct band structure, in contrast to those from the finite-size calculation using NWChem.

TABLE I. Largest absolute values of the NWChem Hamiltonian in a.u. and overlap matrix elements between the next nearest neighbors for different principal layer sizes and basis sets.

No. of atoms in principal layer	LANL2DZ-nw		LANL2DZ-cry	
	Hamiltonian (a.u.)	Overlap	Hamiltonian (a.u.)	Overlap
4	4×10^{-3}	3×10^{-3}	$< 10^{-6}$	$< 10^{-6}$
6	4×10^{-6}	3×10^{-6}	$< 10^{-6}$	$< 10^{-6}$
8	$< 10^{-6}$	$< 10^{-6}$	$< 10^{-6}$	$< 10^{-6}$

We note here that if the unit cell contains only four gold atoms in a Gamma point calculation, the k space sampling in CRYSTAL is not sufficient and we also observed the unphysical band. The importance of k space sampling has been pointed out before.⁵¹ The cluster approximation and the periodic Gamma point calculation show the same incorrect feature in the band structure.

We now turn our attention to the Hamiltonian elements of the finite-size calculations themselves. First, we confirmed that the symmetry $\mathbf{H}_{01} = \mathbf{H}_{12} = \dots$ is fulfilled for principal layer sizes of 4, 6, 8, 10, and 12 for the two basis sets used here (both finite-size and periodic calculations were tested). The situation was different when we looked at the Hamiltonian elements, representing the principal layer itself. Table II gives the largest absolute values of the differences between the Hamiltonian elements of a principal layer and its neighbor for different principal layer sizes from finite-size calculations. We observed that the values do not monotonically decrease with increasing principal layer size. Even though the differences seem smaller for larger systems, the largest absolute value for a principal layer size of 12 atoms for the LANL2DZ-cry basis set is larger than for a principal layer of ten atoms. The assumption that $\mathbf{H}_{00} = \mathbf{H}_{11} = \dots$ is not valid and it appears that increasing the principal layer size does not lead to its fulfillment. In contrast, we found that if periodic boundary conditions are imposed, the absolute values of the differences between the elements of \mathbf{H}_{00} and \mathbf{H}_{11} for the LANL2DZ-cry and the LANL2DZ-nw basis set are below 10^{-6} a.u. for all investigated layer sizes (4–12) and the assumption is valid.

We further investigated the difference between the principal layers by comparing the diagonal contributions to the Hamiltonian and concentrated on a principal layer size of six gold atoms. For larger principal layers, similar results were obtained. The fact that the principal layer condition is fulfilled for a principal layer size of six atoms (see Table I) implies that the overlap between an atom and its reproduction in the neighboring layer can be neglected and, therefore,

TABLE II. Largest absolute values of the differences between the NWCHEM Hamiltonian elements in a.u. of a principal layer and its neighbor and potential differences at layer transition in a.u. measured as the absolute value of the difference between the NWCHEM Hamiltonian projected onto the $5s$ function of the first and the last atom in the principal layer for different principal layer sizes, buffer sizes, and basis sets.

No. of atoms in principal layer	No. of atoms in buffer	Largest Hamiltonian difference (a.u.)		Potential difference (a.u.)	
		LANL2DZ-nw	LANL2DZ-cry	LANL2DZ-nw	LANL2DZ-cry
4	4	1.4×10^{-3}	1.5×10^{-3}	2.9×10^{-3}	3.2×10^{-3}
6	6	1.8×10^{-3}	1.9×10^{-3}	1.6×10^{-3}	5.0×10^{-4}
8	8	1.4×10^{-3}	1.3×10^{-3}	1.1×10^{-4}	5.4×10^{-4}
10	10	8.1×10^{-4}	2.9×10^{-4}	2.5×10^{-4}	5.8×10^{-4}
12	12	2.7×10^{-4}	9.3×10^{-4}	3.5×10^{-4}	5.8×10^{-4}
6	12	7.1×10^{-4}	7.2×10^{-4}	8.9×10^{-4}	7.2×10^{-4}
6	18	2.2×10^{-4}	5.6×10^{-4}	7.0×10^{-5}	5.6×10^{-4}
6	24	3.0×10^{-4}	3.3×10^{-4}	3.4×10^{-4}	3.3×10^{-4}

the kinetic contributions to the Hamiltonian of an atom and its image are equal. In Fig. 4, we plot the projection of the Hamiltonian onto the $5s$ function, measuring the potential around each atom along the gold chain. Note that plotting the projection of the Hamiltonian onto any atomic basis function yields the same qualitative result. Since the kinetic contributions of an atom and its image in the neighboring layer are equal, any inconsistencies between layers are due to an inconsistency in the potential. We observed (Fig. 4) for both basis sets an oscillation in the diagonal $5s$ elements, which is the largest near the end of the chain. In the inset panels, the $5s$ elements of the principal layer and its neighbors are shown. The upper plots [Fig. 4(a)] illustrate the diagonal $5s$ elements for the principal layer approximation by replicating values from atoms 7–12 for atoms 13–18 (repeating itself) which is in contrast to the $5s$ contributions calculated in the finite-size calculation for the entire system shown below [Fig. 4(b)]. For both basis sets used here, the total potential within the principal layer approximation is discontinuous. For the finite calculation, Table II summarizes the difference of the $5s$ elements of the first and the last atom in the principal layer which measures the artificial potential change undergone when translating the principal layer.

When the Hamiltonian is extracted from a periodic calculation of a 24 atom gold chain (lowest plots [Fig. 4(c)]), all gold atoms along the chain are equivalent and there is no inconsistency between layers. This confirms that when periodic boundary conditions are applied and the k -space sampling is converged, the principal layer method can be employed.

We have established that enlarging the principal layer does not eliminate the artificial band. Figure 4 shows that the finite-size effect is concentrated at the ends of the gold chain. To determine if the potential between principal layers is continuous when the buffer size is increased but the principal layer size is kept fixed, we calculated the band structures for a principal layer of six atoms and increased the buffer size to 12, 18, and 24. Using the LANL2DZ-cry basis set in the finite-size calculation shows no artifact in the band structures, but for the LANL2DZ-nw basis set, the artifact appears for a buffer size of 12 and 24 but not for a buffer size of 18 atoms. The differences between \mathbf{H}_{00} and \mathbf{H}_{11} in the

finite-size calculations generally become smaller with increasing system size (Table II). The discontinuities in the potentials at layer transition are also smaller for the larger system (Table II). However, neither the differences nor the discontinuities approach zero for larger systems but rather show oscillating behavior. For a principal layer of 6 atoms and a buffer of 18 atoms (for which we did not observe the

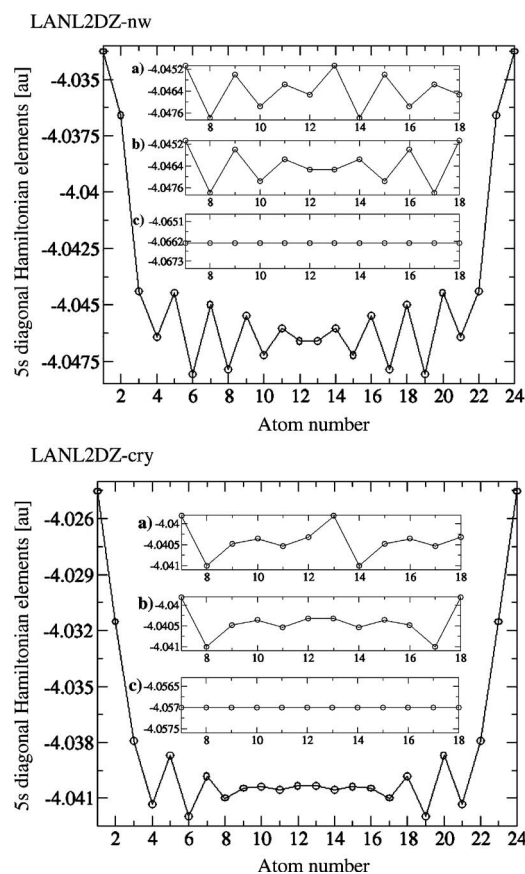


FIG. 4. Hamiltonian projected onto the $5s$ basis function along a 24 atom gold chain, finite-size NWCHEM calculation: Upper panel LANL2DZ-nw and lower panel LANL2DZ-cry. The inset panels enlarge the scale for the Hamiltonian $5s$ elements along atoms 7–18a. (a) Principal layer approximation by replicating values from atoms 7–12 for atoms 13–18. (b) Hamiltonian elements from NWCHEM calculation. (c) Hamiltonian elements from CRYSTAL calculation.

artifact), we observed low values for both criteria when the LANL2DZ-nw basis set was used, but since the artificial band never occurred for the LANL2DZ-cry basis set for which we found larger differences and discontinuities, this observation is inconclusive. In addition, we have tested a symmetric system setup by adding a principal layer and taking \mathbf{H}_{00} and \mathbf{S}_{00} from the center of the chain. This setup also shows the computational artifact.

CONCLUSION

We demonstrated that an unphysical band can appear in the band structure when the cluster approximation is used in combination with the principal layer method for the example of a one-dimensional gold chain. The existence of the artifact depends on the basis set used and on the sampling of the Brillouin zone (when periodic conditions are applied). Very small changes in the basis set cause the artificial band. For example, the most diffuse s function in the LANL2DZ-nw basis has an exponent of 0.060 and the most diffuse p function of 0.028. The less diffuse but otherwise the same basis set LANL2DZ-cry, for which we did not see the additional band, has an exponent of 0.098 for the most diffuse p function and 0.080 for the most diffuse s function. Increasing the principal layer size does not lead to the disappearance of the artifact. In addition, the increase in the buffer size is only partly successful. For the principal layer method to be applicable the assumption that $\mathbf{H}_{00}=\mathbf{H}_{11}=\dots$ needs to be valid and the potential needs to transition smoothly between layers. Both criteria are violated for the basis set for which we observe the artifact but also for the basis for which we do not. Oscillations in the potential along the finite gold chain which is used to obtain the Hamiltonian and overlap matrices for transport calculations cause a discontinuity in the potential of the semi-infinite leads when the principal layer method is applied. If the principal layer method is applied in combination with a periodic calculation for the Hamiltonian using a converged sampling of the Brillouin zone, the assumption $\mathbf{H}_{00}=\mathbf{H}_{11}=\dots$ is verified and the potential is shown to be smooth at layer transition. As a result, there is no additional unphysical band appearing for either atomic orbital basis set. While a clear quantitative measure for the onset of the appearance of the unphysical behavior was not described, our investigations underline the importance of comparing the band structure obtained from periodic calculations (or experiments) to that obtained using input from cluster calculations before proceeding with the description of complex devices.

ACKNOWLEDGMENTS

This research was supported by the Division of Chemical Sciences, Geosciences, and Biosciences, Office of Basis Energy Sciences, U.S. Department of Energy, under Contract No. DE-AC05-00OR22725 with Oak Ridge National Laboratory, managed and operated by UT-Battelle, LLC, and, in part, by ORNL Laboratory Directed Research and Development Funds.

- ¹X. Xiao, B. Xu, and N. J. Tao, *Nano Lett.* **4**, 267 (2004).
- ²V. B. Engelkes, J. M. Beebe, and C. D. Frisbie, *J. Am. Chem. Soc.* **126**, 14287 (2004).
- ³V. Burtman, A. S. Ndobé, and Z. V. Vardeny, *J. Appl. Phys.* **98**, 034314 (2005).
- ⁴M. A. Reed, C. Zhou, C. J. Muller, T. P. Burgin, and J. M. Tour, *Science* **278**, 252 (1997).
- ⁵M. P. Samanta, W. Tian, S. Datta, J. I. Henderson, and C. P. Kubiak, *Phys. Rev. B* **53**, R7626 (1996).
- ⁶E. G. Emberly and G. Kirczenow, *Phys. Rev. B* **58**, 10911 (1998).
- ⁷L. E. Hall, J. R. Reimers, N. S. Hush, and K. Silverbrook, *J. Chem. Phys.* **112**, 1510 (2000).
- ⁸M. Di Ventra, S. T. Pantelides, and N. D. Lang, *Phys. Rev. Lett.* **84**, 979 (2000).
- ⁹P. A. Derosa and J. M. Seminario, *J. Phys. Chem. B* **105**, 471 (2001).
- ¹⁰Y. Xue, S. Datta, and M. A. Ratner, *J. Chem. Phys.* **115**, 4292 (2001).
- ¹¹C.-K. Wang, Y. Fu, and Y. Luo, *Phys. Chem. Chem. Phys.* **3**, 5017 (2001).
- ¹²K. Stokbro, J. Taylor, M. Brandbyge, J.-L. Mozos, and P. Ordejón, *Comput. Mater. Sci.* **27**, 151 (2003).
- ¹³J. Tomfohr and O. F. Sankey, *J. Chem. Phys.* **120**, 1542 (2004).
- ¹⁴S.-H. Ke, H. U. Baranger, and W. Yang, *Phys. Rev. B* **71**, 113401 (2005).
- ¹⁵W. Tian, S. Datta, S. Hong, R. Reifenberger, J. I. Henderson, and C. P. Kubiak, *J. Chem. Phys.* **109**, 2874 (1998).
- ¹⁶S. N. Yaliraki, A. E. Roitberg, C. Gonzalez, and M. A. Ratner, *J. Chem. Phys.* **111**, 6997 (1999).
- ¹⁷F. Remacle and R. D. Levine, *Appl. Phys. Lett.* **85**, 1725 (2004).
- ¹⁸M. Kondo, T. Tada, and K. Yoshizawa, *Chem. Phys. Lett.* **412**, 55 (2005).
- ¹⁹E. G. Emberly and G. Kirczenow, *Phys. Rev. Lett.* **91**, 188301 (2003).
- ²⁰A. M. Bratkovsky and P. E. Kornilovitch, *Phys. Rev. B* **67**, 115307 (2003).
- ²¹E. G. Emberly and G. Kirczenow, *Phys. Rev. B* **64**, 235412 (2001).
- ²²H. Geng, S. Yin, K.-Q. Chen, and Z. Shuai, *J. Phys. Chem. B* **109**, 12304 (2005).
- ²³C. Toher, A. Filippetti, S. Sanvito, and K. Burke, *Phys. Rev. Lett.* **95**, 146402 (2005).
- ²⁴S. Kurth, G. Stefanucci, C.-O. Almbladh, A. Rubio, and E. K. U. Gross, *Phys. Rev. B* **72**, 035308 (2005).
- ²⁵X. Qian, J. Li, X. Lin, and S. Yip, *Phys. Rev. B* **73**, 035408 (2006).
- ²⁶G. C. Solomon, J. R. Reimers, and N. S. Hush, *J. Chem. Phys.* **121**, 6615 (2004).
- ²⁷A. Ferretti, A. Calzolari, R. Di Felice, F. Manghi, M. J. Caldas, M. Buongiorno Nardelli, and E. Molinari, *Phys. Rev. Lett.* **94**, 116802 (2005).
- ²⁸K. Burke, M. Koentopp, and F. Evers, *Phys. Rev. B* **73**, 121403 (2006).
- ²⁹Y.-C. Chen, M. Zwolak, and M. Di Ventra, *Nano Lett.* **4**, 1709 (2004).
- ³⁰R. Landauer, *Phys. Lett. A* **85**, 91 (1981).
- ³¹N. D. Lang, *Phys. Rev. B* **52**, 5335 (1995).
- ³²S. Datta, *Electronic Transport in Mesoscopic Systems* (Cambridge University Press, Cambridge, 1995).
- ³³V. Mujica, M. Kemp, and M. A. Ratner, *J. Chem. Phys.* **101**, 6849 (1994).
- ³⁴V. Mujica, M. Kemp, and M. A. Ratner, *J. Chem. Phys.* **101**, 6856 (1994).
- ³⁵M. Brandbyge, J.-L. Mozos, P. Ordejón, J. Taylor, and K. Stokbro, *Phys. Rev. B* **65**, 165401 (2002).
- ³⁶A. Calzolari, N. Marzari, I. Souza, and M. Buongiorno Nardelli, *Phys. Rev. B* **69**, 035108 (2004).
- ³⁷E. Apra *et al.*, NWChem, A Computational Chemistry Package for Parallel Computers, version 4.7, Pacific Northwest National Laboratory, Richland, Washington 99352-0999, USA, 2005.
- ³⁸W. C. Lu, V. Meunier, and J. Bernholc, *Phys. Rev. Lett.* **95**, 206805 (2005).
- ³⁹V. Meunier and B. G. Sumpter, *J. Chem. Phys.* **123**, 024705 (2005).
- ⁴⁰V. Meunier, W. C. Lu, B. G. Sumpter, and J. Bernholc, *Int. J. Quantum Chem.* **106**, 3334 (2006).
- ⁴¹M. Fuentes-Cabrera, V. Meunier, and B. G. Sumpter, *Nanotechnology* **18**, 424019 (2007).
- ⁴²V. Meunier, S. V. Kalinin, and B. G. Sumpter, *Phys. Rev. Lett.* **98**, 056401 (2007).
- ⁴³Y. Xue, S. Datta, and M. A. Ratner, *Chem. Phys.* **281**, 151 (2002).
- ⁴⁴M. B. Nardelli, *Phys. Rev. B* **60**, 7828 (1999).
- ⁴⁵M. P. López Sancho, J. M. López Sancho, and J. Rubio, *J. Phys. F: Met.*

[Phys.](#) **15**, 851 (1985).

⁴⁶C. Pisani and R. Dovesi, [Int. J. Quantum Chem.](#) **17**, 501 (1980).

⁴⁷J. C. Slater and K. H. Johnson, [Phys. Rev. B](#) **5**, 844 (1972).

⁴⁸S. J. Vosko, L. Wilk, and M. Nusair, [Can. J. Phys.](#) **58**, 1200 (1980).

⁴⁹A. Calzolari, C. Cavazzoni, and M. Buongiorno Nardelli, [Phys. Rev. Lett.](#) **93**, 096404 (2004).

⁵⁰H. J. Monkhorst and J. D. Pack, [Phys. Rev. B](#) **13**, 5188 (1976).

⁵¹K. S. Thygesen and K. W. Jacobson, [Phys. Rev. B](#) **72**, 033401 (2005).